

<https://doi.org/10.1038/s41612-025-01084-y>

The response of AUSM to precession forcing and its relation to EASM and EAWM

Mi Yan^{1,2}, Zhengyu Liu³, Bin Wang⁴, Xinwei Kong¹, Liang Ning^{1,2}, Qin Wen^{1,2} & Jian Liu^{1,5} ✉

The East Asian monsoon (EAM) and the Australian monsoon (AUM), which constitute the two subsystems of the Asian–Australian monsoon system, are dynamically linked through cross-equatorial flows while also responding distinctly to external forcings. Although previous studies have examined their relationships across various timescales, their connection at the orbital timescale remains underexplored. Through a series of simulations, we demonstrate that Australian Summer Monsoon (AUSM) precipitation varies out of phase with East Asian Summer Monsoon (EASM) precipitation at the precession timescale due to local insolation changes. At the same timescale, the relationship between AUSM circulation and East Asian winter monsoon (EAWM) circulation is weak. This weak linkage arises from the precession-induced inter-hemispheric insolation gradient, which diminishes cross-equatorial flow and consequently weakens the dynamical links between AUSM and EAWM circulations.

The Asian–Australian monsoon system comprises three sub-monsoon systems: the Australian monsoon (AUM), the South Asian monsoon (SAM), and the East Asian monsoon (EAM). Each sub-monsoon system can show distinct changes in response to external forcing and internal variability (e.g., sea surface temperature (SST))^{1,2}. Furthermore, the EAM and AUM can interact with each other through cross-equatorial flow around the Maritime Continent³.

Proxy reconstructions and climate model simulations have demonstrated that the relationship between East Asian summer monsoon (EASM) precipitation and Australian summer monsoon (AUSM) precipitation is not consistent across timescales, due to their differing responses to external forcings and internal variations^{4–6}. At the precession timescale, there is an ongoing debate about whether the strengths of AUSM and EASM vary “in-phase”^{1,7,8} or “out-of-phase”^{9,10}. This debate underscores a long-standing uncertainty regarding the causes of changes in AUSM⁷: Are the changes in AUSM driven by local austral summer insolation over Australia or by remote boreal winter insolation over Asia?

Theoretically, the seasonality of the precession-induced insolation changes in opposite directions between the Northern Hemisphere (NH) and Southern Hemisphere (SH). For instance, at a minimum precession, the NH and SH receive more insolation for boreal summer (austral winter) and less insolation in boreal winter (austral summer). The increased insolation in

boreal summer will lead to a strengthened EASM¹¹ (Wen et al. 2016), while the decreased insolation in austral summer tends to weaken the AUSM. Therefore, if the monsoon systems are determined predominantly by local insolation forcing, the opposite change of local summer monsoon over NH and SH should force an out-of-phase variation at the precession scale, i.e., a negative (or “out-of-phase”) relationship between the AUSM and the EASM. This precession-induced interhemispheric out-of-phase monsoon intensity was supported by some proxies from the Asian cave speleothem record, the North African dust record, and the South American cave speleothem record. Records from Australia, however, have not yet provided absolutely dated evidence for the out-of-phasing to the NH monsoons¹².

On the other hand, the AUSM is believed to be connected to the East Asian winter monsoon (EAWM) through cross-equatorial flow¹³. A strong EAWM may enhance the cross-equatorial outflow, the convergence over the Australian monsoon region, and consequently, the AUSM precipitation. The reconstructions by Clemens et al.¹⁴ and Sun et al.¹⁵ indicate that the EASM and EAWM variations were in phase at precession timescales, prior to the significant Northern Hemisphere glacial cycles approximately 3 million years ago. This in-phase relationship between the EAWM and the EASM at precession timescales has been observed in some recent modeling studies, which were solely influenced by orbital forcing^{11,16,17}. If the local insolation-induced AUSM variation is dominated by the remote dynamical

¹State Key Laboratory of Climate System Prediction and Risk Management, Key Laboratory for Virtual Geographic Environment, State Key Laboratory Cultivation Base of Geographical Environment Evolution of Jiangsu Province, Jiangsu Center for Collaborative Innovation in Geographical Information Resource Development and Application, School of Geography, Nanjing Normal University, Nanjing, China. ²State Key Laboratory of Loess and Quaternary Geology, Institute of Earth Environment, CAS, Xi'an, China. ³Department of Geography, The Ohio State University, Columbus, OH, USA. ⁴Department of Atmospheric Sciences, University of Hawai'i at Manoa, Honolulu, HI, USA. ⁵Jiangsu Provincial Key Laboratory for Numerical Simulation of Large Scale Complex System, School of Mathematical Science, Nanjing Normal University, Nanjing, China. ✉e-mail: jlju@njnu.edu.cn

forcing from the EAWM, we should anticipate a positive (or “in-phase”) relationship between AUSM precipitation and EASM precipitation at precession timescales. However, the sensitivity of the AUSM to the inter-hemispheric interaction with the EAWM remains a topic of intense debate due to a limited understanding of past variability and conflicting results from simulations and reconstructions^{1,8,18,19}.

Recently, some new records have been reconstructed to reflect the Australian climate evolution during the past 300–400 kyrs^{20–22}, which provide opportunities to better understand the EAM–AUM relationship. However, they have not been used to quantitatively investigate the EASM–AUSM relationship at the precession timescale, which, therefore, remains unsolved. We then raise the following questions: What is the relationship between the AUSM and the EASM at the precession timescale forced by the precession? Is the AUSM predominated by the local insolation or dynamically linked to the EAWM? In this study, we investigate the relationship between the EAM and AUM at the precessional timescale over the past 300,000 years (300 kyrs) in a numerical model simulation. The monsoon intensity is defined from both pre-

cipitation and circulation perspectives. The strengthened summer monsoon intensity is corresponded to the increased monsoon precipitation. The strengthened EASM/EAWM is accompanied with the increased regional low-level southerly/northerly. The strengthened AUSM is accompanied with the increased regional low-level westerly. Specifically, we mainly discuss the monsoon precipitation in local summer for the summer monsoons’ relationship and the monsoon circulation in austral summer to find out the dynamical link. It was found that local precession-induced insolation plays a dominant role in modulating the relationships between the EAM and the AUM. Local SST and remote insolation may also have modulation effects. We first compare the relationship between the summer monsoon precipitation of AUSM and EASM, along with the possible mechanisms. Then, we investigate the simultaneous dynamic linkage between the AUSM circulation and the EAWM circulation and its possible mechanisms. Thirdly, we discuss the other processes that may have modulation roles and provide some model-model and model-data comparisons. The last section provides the conclusions.

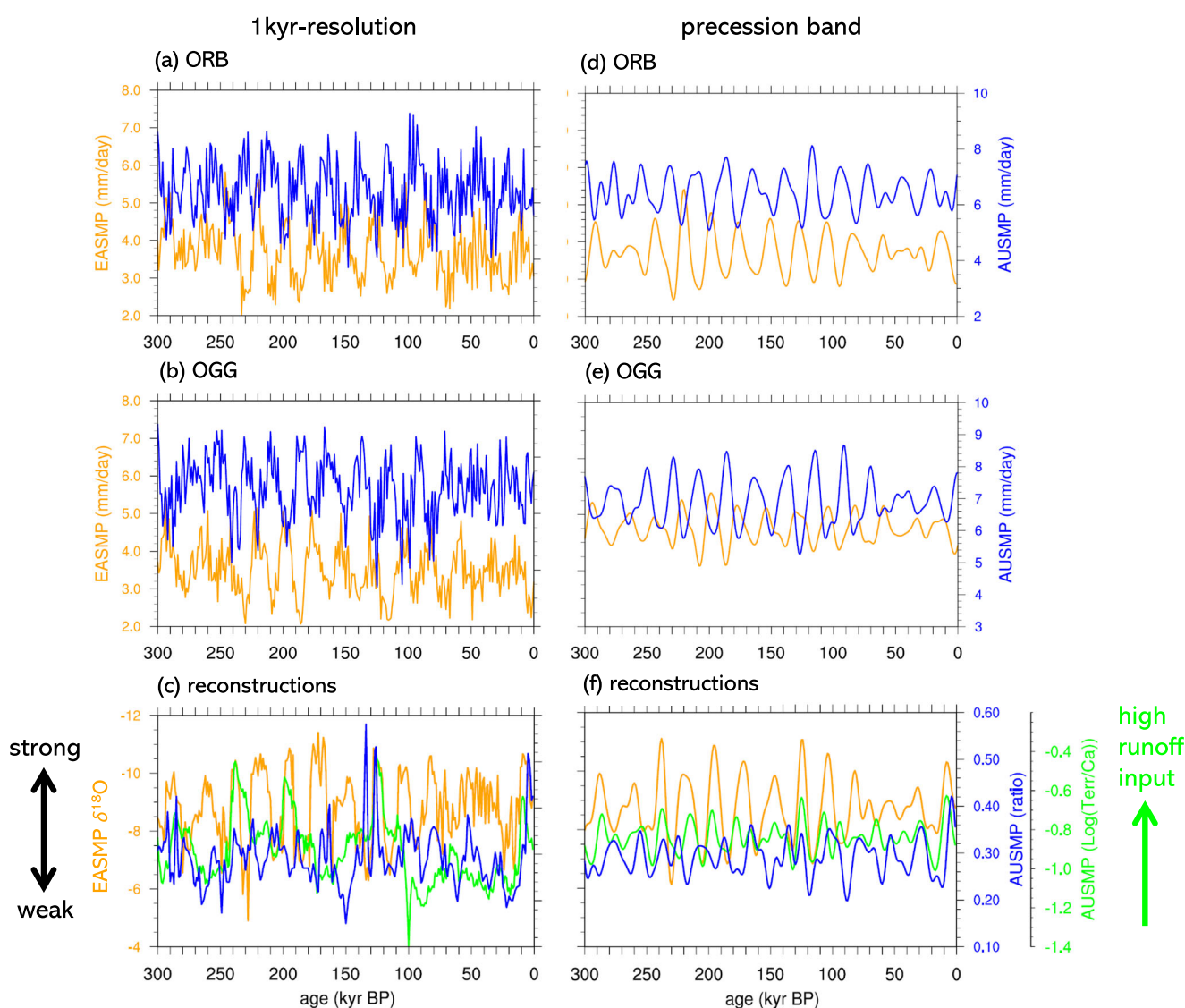
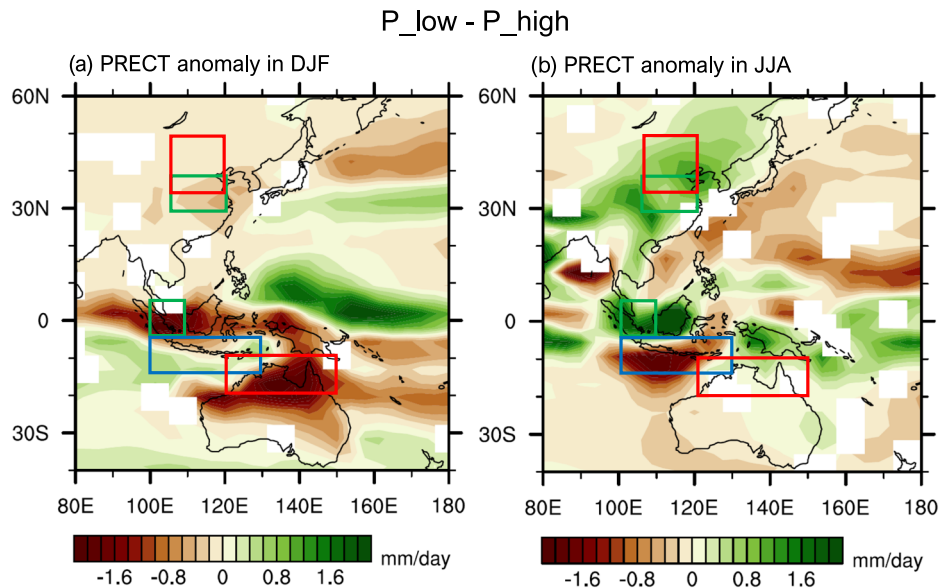


Fig. 1 | Temporal evolution of EASM and AUSM over the past 300,000 years. Time series of (a, b, d, e) simulated and (c, f) reconstructed EASM (orange) and AUSM (blue) precipitation over the past 300,000 years (300 kyr). The EASM proxy (orange line in c, f) is the composite $\delta^{18}\text{O}$ records from Chinese caves reconstructed by Cheng et al.²⁴. The AUSM proxies are the kaolinite/smectite ratio from IODP site

U1483 reconstructed by Sarim et al.²¹ (blue line in c, f), and the monsoonal discharge ($\text{Log}(\text{Terr}/\text{Ca})$) record integrated from Core SO257-18548 and IODP site U1482 by Pei et al.²⁰ (green line in c, f). Shown are the time series with 1-kyr resolution (left panels) and in their precession band (right panels). The simulated results are derived from pure orbital run (ORB, a, d) and three forcings run (OGG, b, e).

Fig. 2 | Precipitation changes between the low and high precession states. The composite maps of total precipitation rate (PRECT) anomalies in DJF (a) and in JJA (b). The differences are obtained between the low and high precession states ($P_{low} - P_{high}$). Only those values above 95% confidence level are shown. The color boxes illustrate the regions used to define the indices for the following section. In green boxes, the meridional wind is used. In blue boxes, the zonal wind is used. In red boxes, the precipitation is used.



Results

The out-of-phase relationship between AUSM and EASM

Here, we show the time series of the AUSM precipitation and EASM precipitation in the pure orbital experiment, which is only forced by the transient orbital parameters (ORB), along with those in the realistic experiment, which is forced by orbital, greenhouse gases and ice sheet (OGG) (Fig. 1a, b). The experiments are conducted using the Community Climate System Model version 3 (CCSM3). The details of the experiments can be found in Lu et al.²³ and the Method section. The simulated EASM precipitation is defined as the area averaged June–July–August (JJA) mean precipitation over northern China (35°N–50°N, 105°E–120°E). The simulated AUSM precipitation is defined as the area averaged December–January–February (DJF) mean precipitation over northern Australia over land (20°S–10°S, 120°E–150°E).

Two proxy-based monsoon indices representing EASM²⁴ and AUSM²¹ (Fig. 1c) are used to evaluate our simulated results. The composite $\delta^{18}O$ records from Chinese caves reconstructed by Cheng et al.²⁴ have been widely used to represent the EASM. Sarim et al.²¹ collected high-resolution clay mineral assemblages and siliciclastic grain-size records from the International Ocean Discovery Program (IODP) site U1483, in which the Kaolinite/smectite ratios were adopted as the proxy for the AUSM. A high kaolinite/smectite ratio indicates a strong AUSM. Another record representing the AUSM intensity reconstructed by Pei et al.²⁰ is also adopted. In Pei et al.²⁰, the AUSM intensity was represented by the monsoonal discharge ($\text{Log}(\text{Terr}/\text{Ca})$) in a composite record from Core SO157-18548 and IODP site U1482. A large $\text{Log}(\text{Terr}/\text{Ca})$ value indicated a high runoff input by monsoonal discharge, i.e., a stronger AUSM.

It is clear that the simulated EASM and AUSM precipitation are predominated with precession signal and vary oppositely (Fig. 1). They show significant anti-phase coherence at the precession band with a $\sim 180^\circ$ phase shift. The correlation coefficient at lag-0 is -0.73 at the precession timescale between the filtered simulated EASM precipitation and the AUSM precipitation in the ORB run. The out-of-phase relationship between the AUSM and the EASM is robust in the pure orbital run (ORB, Fig. 1a) and in the realistic run (OGG, Fig. 1b).

However, there is uncertainty in the reconstructed AUSM-EASM relationship. The AUSM intensity reconstructed by Sarim et al.²¹ exhibits a clear anti-phase variation compared to the reconstructed EASM (blue line vs. orange line in Fig. 1c), while the AUSM intensity reconstructed by Pei et al.²⁰ demonstrates a roughly in-phase variation with the reconstructed EASM (green line vs. orange line in Fig. 1c). We then calculated the correlation coefficient at lag-0 between the AUSM

reconstructed by Pei et al.²⁰ and the EASM reconstructed by Cheng et al.²⁴ at their precession band, which is positive with a value of 0.55 (not significant). It is important to note that while the AUSM indicated by Sarim et al.²¹ shows an anti-phase variation relative to the EASM indicated by Cheng et al.²⁴, their correlation coefficient at lag-0 on the precession timescale is -0.06 , which is not significant. The inconsistency between the two AUSM proxies reflects a similar proxy inconsistency noted in previous works⁸. This highlights the uncertainty of proxy records in accurately representing the AUSM. Here, we endeavor to determine whether the proxies and the inferred monsoon responses can be understood physically within the context of our model.

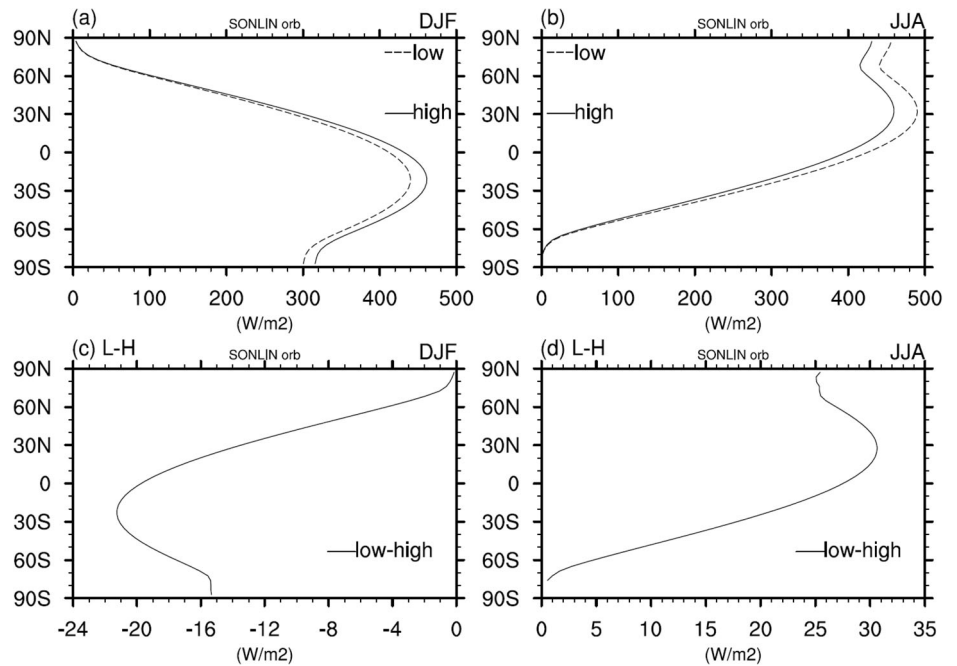
The composite analysis of maps (Fig. 2) and seasonal cycles (Fig. S1) shows that at the low precession stages, the AUSM precipitation over the land is decreased (Figs. 2a, S1a), whereas the EASM precipitation is increased (Figs. 2b, S1b). This also illustrates an “out-of-phase” relationship between the AUSM and the EASM. Note that the AUSM precipitation over the adjacent ocean is increased. We then suggest that if the reconstructed AUSM represents the signal over the ocean, it could be expected a positive relationship with the EASM, shown, for example, in the relationship between Pei et al.²⁰ and Cheng et al.²⁴. We noticed that, dominated by the JJA negative anomaly, the annual mean precipitation over the adjacent ocean also decreased (Figure S2c). The opposite precipitation changes over land and ocean near northwest Australia are also presented in a previous simulation work by Liu et al.¹ using another coupled ocean-atmosphere model (FOAM). However, the relative magnitudes of the opposite changes differ potentially due to model dependence.

Previous reconstructions have suggested that the tropical precipitation pattern could be explained by an interhemispheric anti-phase pattern at the precession timescale, which was related to the monsoon intensity modulated by the precession-induced inter-hemispheric contrast insolation between NH and SH^{25,26}. This agrees with our simulated result that the AUSM and EASM precipitation have out-of-phase variations at the precession timescale. Such an out-of-phase relationship indicates that the AUSM and the EASM might be dominated by the local precession-induced insolation, and there might be a weak dynamical linkage between the EASM and the AUSM.

Local insolation dominates the out-of-phase relationship between AUSM and EASM

Reconstruction works have proposed that the monsoon evolution at orbital timescales followed the orbital-induced insolation closely²⁷. Our previous simulation works also revealed the important role of the local and remote

Fig. 3 | Meridional distribution of zonal mean insolation at top of atmosphere. Composite maps of zonal mean insolation at the top of atmosphere (SOLIN) climatology at high (solid line) and low (dashed line) precession stages (a, b) and its anomalies (c, d) in DJF (a, c) and JJA (b, d). The composite anomalies are the differences between low and high precession states (L-H).



orbital-induced insolation on the Asian and Australian monsoon changes in the Holocene^{28,29}.

The precession-induced insolation tends to warm/cool the NH and SH in the same direction (Fig. 3c, d). From the energy point of view, the moist static energy (MSE) at low levels, including near surface (Fig. S3) and 850 hPa (Fig. 4a, d), reduced/increased over most parts of the globe in DJF/JJA in response to the reduced/increased insolation at low precession stages. The reduced MSE over the Australian continent in DJF (Fig. 4a) directly leads to the reduced AUSM precipitation (Fig. 2a). In contrast, the increased MSE over the East Asia in JJA (Figs. S3b, 4d) leads to the increased EASM precipitation (Fig. 2b).

Note the peculiar increased surface temperature over the northern Australian continent in DJF (Fig. 4b), and it doesn't seem to match the increased SLP and the anomalous anti-cyclone wind at 850 hPa (Fig. 4c, similar to surface wind), and, in turn, the reduced monsoon precipitation (Fig. 2a). Instead, it is consistent with the minimum MSE (Figs. 4a, S3a), implying that a dry condition accompanies the warming. Decreased precipitation may lead to a drier surface and warmer temperature³⁰. Thus, this land warming might be the result, rather than the cause, of the reduced AUSM precipitation over land. Therefore, we argue that the precession-induced reduction of local insolation directly dominates the reduced AUSM precipitation and the resulting low MSE.

Regarding the strengthened EASM at low precession stages, besides the increased MSE (Figs. 4d, S3b), the surface temperature increases more over the land than over the ocean, leading to increased land-sea thermal contrast (Fig. 4e) and thus the increased land-sea SLP contrast and, in turn, the strengthened EASM southerly (Fig. 4f) and northward moisture transport. Such local processes in the EASM region play a dominant role in enhancing the intensity of EASM with enhanced rainfall, especially in northern China. Meanwhile, the northward cross-equatorial flow is also strengthened. This may imply an additional remote impact that enhances the EASM from the SH.

Quantification of the simultaneous dynamical link between AUSM and EASM

The composite results revealed by our transient simulation is consistent with the previous results derived from a series of equilibrium simulations forced by different obliquity-precession configurations³¹. In their experiments, the reduction in local summer insolation associated with a “high precession”

(their “high precession” indicates NH precession, i.e., our “low precession”) led to a lowered precipitation rate over most monsoon regions of northern Australia, accompanied by an increased precipitation rate over Maritime Continent, even though the EAWM wind towards the equator is enhanced. These modeling simulations lead us to hypothesize that the simultaneous dynamical link between the EAWM and the AUSM can be weakened, or even overwhelmed by the local response to precessional forcing.

To quantitatively assess the simultaneous dynamical links between the EAM and the AUM, we defined three circulation indices: the meridional wind over EAM region (30°–40°N, 105°–120°E), the meridional wind over Maritime Continent (5°S–5°N, 100°–110°E) (green boxes in Fig. 2) and the zonal wind over AUM region (15°S–5°S, 100°–130°E) (blue boxes in Fig. 2). The meridional wind and zonal wind at 850 hPa geopotential height are used. The JJA mean and DJF mean meridional wind over the EAM region are used to represent the EASM and EAWM circulation intensities, respectively (EASM_v850, EAWM_v850). The meridional wind over the Maritime Continent is used as a proxy of cross-equatorial flow. The DJF mean zonal wind over the AUM region is used to illustrate the AUSM circulation intensity (AUSM_u850). Since the DJF mean zonal wind corresponding to the AUSM circulation is a westerly wind, we refer to it as “AUSM westerly” in the following part. The rainfall indices are the above-mentioned summer monsoon precipitation of EASM (EASM_P) and AUSM (AUSM_P, over land only).

In this study, the EAWM and the AUSM are regarded as dynamically linked if they both have a positive (or “in-phase”) simultaneous relationship with the cross-equatorial flow. The correlation coefficient at lag-0 and the phase shift at the precession timescale between each index are listed in Table 1.

In boreal winter (DJF), although the EAWM northerly is significantly positively correlated with the cross-equatorial flow, with a near 0° phase shift, the correlation coefficients are small and insignificant between the AUSM westerly and the cross-equatorial flow and between the AUSM westerly and the EAWM northerly. This confirms our hypothesis of the weak dynamical link between the EAWM and the AUSM.

This hypothesis is also consistent with the significant nearly out-of-phase coherence between the AUSM_P and the EAWM_v850, along with the insignificant negative correlation coefficient (−0.40 in Table 1). This suggests that the AUSM circulation and precipitation might be influenced predominantly by other mechanisms instead of the dynamical process from

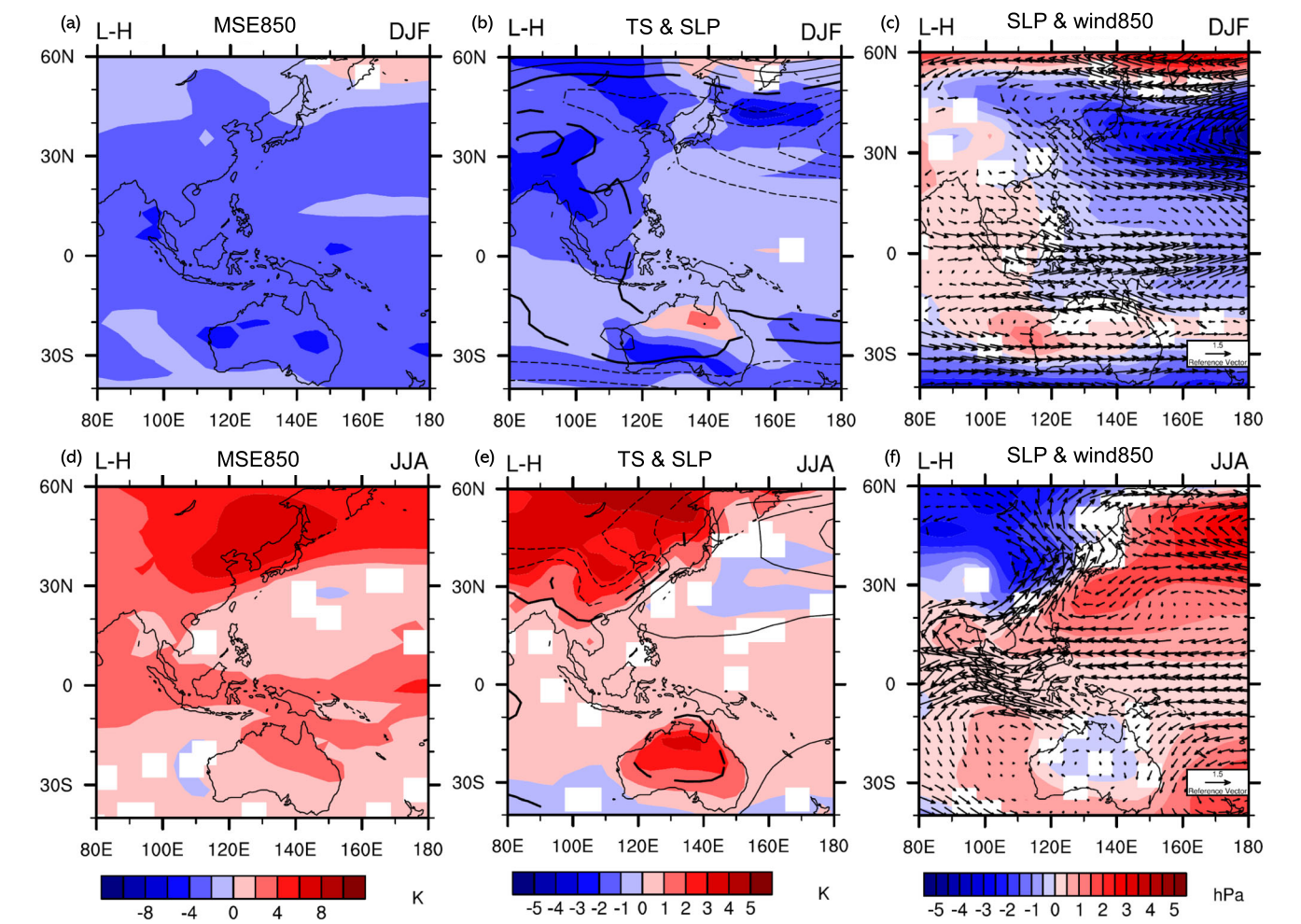


Fig. 4 | Characteristics of surface and low-level climate changes. Composite maps of (a, d) moist static energy at 850 hPa (MSE850) and (b, e) surface temperature (TS, shading) along with sea level pressure (SLP, contour), and (c, f) SLP (shading) along with wind at 850 hPa (vector) anomalies in DJF (a–c) and JJA (d–f). The composite anomalies are the differences between low and high precession states. Only those values above 95% confidence level are shown. The results are derived from ORB run.

Table 1 | The correlation coefficient at lag-0 and the phase shift between each index

Index	Lag-0 correlation coefficient	Phase shift (°)
EAWM_v850 vs. Cross-equatorial flow	0.70*	10#
AUSM_u850 vs. -Cross-equatorial flow	0.16	–100
AUSM_u850 vs. -EAWM_v850	–0.13	–122
AUSM_P vs. -EAWM_v850	–0.40	138#

The results are derived from the ORB run. The correlation coefficient between each index is conducted based on their filtered precession band. An asterisk (*) indicates the correlation coefficient being above the 90% confidence level, as determined by applying the Monte Carlo test. A pound (#) indicates the phase in which the coherence square passed the 90% confidence level in the coherence analysis.

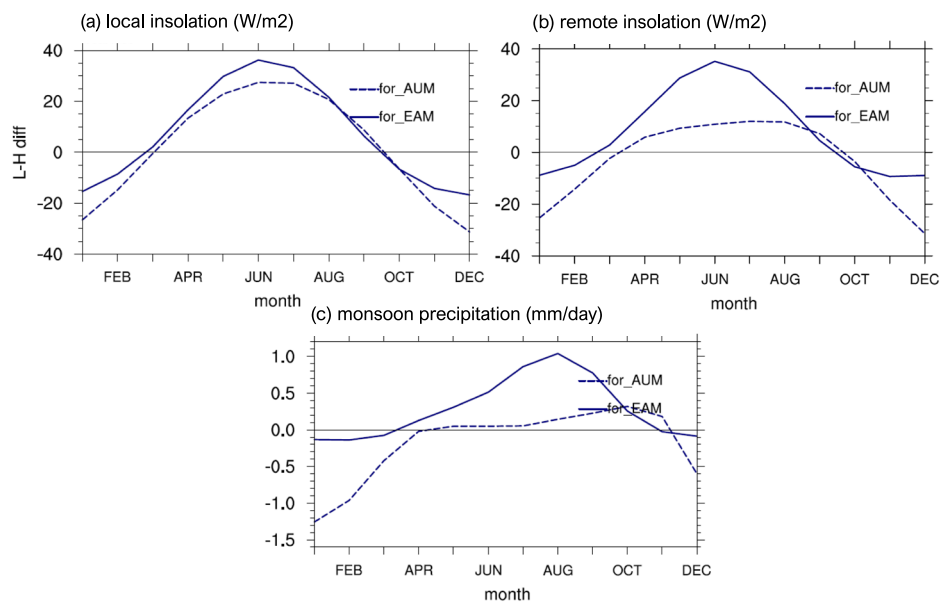
the NH. In other words, the remote AUSM-EAWM dynamic linkage might be overwhelmed by the local insolation-induced effect for the precessional forcing.

To summarize, our model simulations suggest that the dynamic link between the EAWM and the AUSM is weak at the precession timescale (insignificant -0.13 correlation coefficient in Table 1). The relationships between each index still hold after being imposed with GHGs and ice sheets (figures not shown), suggesting limited roles of GHGs and ice sheets on the precessional time scale in our model. The roles of GHGs and ice sheets in modulating the monsoon dynamics are beyond the scope of this paper and will be discussed elsewhere.

The hemispheric insolation gradient regulates the interhemispheric dynamical links

Although the precession induced insolation cooling/warming is of the same sign, or in the same direction, in both the NH and SH, the magnitude of the change is different across latitudes. At low precession stages, the insolation in DJF reduces more over the SH, especially the mid-low latitude, than over the NH (Fig. 3c). The SH-NH insolation gradient over mid-low latitude (from 30S to 30N) is reduced by 5%, from $2.27 \times 10^{-2} \text{ W/m}^2/\text{km}$ to $2.16 \times 10^{-2} \text{ W/m}^2/\text{km}$. The reduced SH-NH insolation gradient leads to weakened interhemispheric contrast in temperature and SLP over the low latitudes (shading in Figs. 4c, and S4). The weakened north-south SLP

Fig. 5 | Seasonal cycles of insolation and monsoon precipitation. Composite seasonal cycles of insolation at top of atmosphere anomalies (a, b) and precipitation anomalies in monsoon regions (c). The composite anomalies are differences between low and high precession stages. (a) shows the related local insolation for EAM (30°N–40°N) and for AUM (15°S–5°S). (b) shows the related remote insolation for EAM (45°N–60°N) and for AUM (60°S–30°S).



gradient (Fig. S4c) then weakens the tropical easterly and, in turn, the cross-equatorial flow from NH to SH. As such, the remote dynamical impact of the EAWM on AUSM is weakened. The weakened AUSM westerly and the reduced AUSM precipitation is caused by the local south-north SLP gradient between the Australian continent and the nearby ocean to the north, which is reversed and induces an anomalous easterly over the Australian monsoon region, exporting moisture away from the Australian continent into the nearby ocean to the northeast, decreasing rainfall over land and increasing rainfall over the ocean (vector in Fig. 4c).

In JJA, on the other hand, although the insolation increases globally at low precession stages, the mid-low latitudes over the NH receives more insolation than other regions (Fig. 3d). The NH-SH insolation gradient over mid-low latitude (from 30°S to 30°N) increases by 6% from 3.13×10^{-2} W/m²/km to 3.32×10^{-2} W/m²/km. The increased NH-SH insolation gradient strengthens the SH-NH SLP gradient (Fig. S4d), the northward cross-equatorial flow, and the remote dynamic link between the SH circulation and the EASM.

In short, caused by the precession-induced changes of the insolation gradient between SH and NH over mid-low latitude, the dynamical link between the EAWM and the AUSM is weakened or even “cut off” at the precession timescale.

Discussions

Wen et al.²⁸ studied the responses of EAWM and AUSM to local and remote orbital forcing during the Holocene in model simulations that apply anomalous insolation forcing in different latitude bands. They found that the local forcing for AUSM was overwhelmed by remote forcing from both NH low latitude and SH high latitude. Our composite results of the seasonal cycle of local and remote insolation and precipitation in monsoon regions (Fig. 5) suggest that the AUSM precipitation is influenced by both local (15°S–5°S) and remote extratropical SH (60°S–30°S) insolation (Fig. 5c). The EASM precipitation is also affected by local (30°N–40°N) and remote extratropical NH (45°N–60°N) insolation, which is consistent with our previous work²⁹. We notice that the EASM precipitation peaks in August, two months after the insolation peak; this might be due to the selected region that defines the monsoon precipitation. We use the precipitation over northern China, where the precipitation peaks in August, to represent the EASM precipitation, and the August peak is related to the seasonal migration of the EASM circulation.

Here, we note that the impacts of local and remote forcing are assessed by comparing the seasonal cycle of insolation at different latitude bands to

that of the precipitation over the monsoon region. The insolation represents the local insolation for EASM (30°N–40°N), and the local insolation for AUSM is represented by the insolation over (15°S–5°S). The remote insolation for EASM is represented by the insolation over (45°N–60°N), and the remote insolation for AUSM is represented by the insolation over (60°S–30°S). This assessment may not be accurate because, first, the seasonal cycles of insolation at different latitudes are not completely independent, and second, the monsoon responses to localized insolation forcing may not be linear. Therefore, transient sensitivity experiments with insolation forcing in different latitude bands, similar to Wen et al.²⁸, are required in the future to quantitatively isolate the roles of the local and remote insolation on the monsoon evolutions more precisely.

By comparing the evolution of global monsoons during Holocene in both a coupled climate model and a coupled AGCM-slab ocean model, Liu et al.¹ found that the direct insolation forcing of the EAWM alone was insufficient to enhance the Australian monsoon. Instead, the local oceanic dynamic response also plays an important role, particularly in AUSM.

Here, we cannot explicitly isolate the role of oceanic dynamics, as we do not have a parallel transient simulation in an uncoupled model. Alternatively, we compare the changes in monsoon activities during transition seasons when the orbital-induced insolation is minimal. The variations in precession-induced insolation in March and October are relatively small (Fig. 6a, b). However, the changes in monsoon circulation and precipitation in March (October) (Fig. S5) resemble those in DJF (JJA) as shown in Fig. 2. The differing responses between March and October may be related to the observation that the SST in March (October) (Fig. 6c, d) is similar to that in DJF (JJA) (figures not shown). This confirms the role of SST in modulating the responses of EAM and AUM to orbital-induced insolation, even though these SST effects encompass both thermo and dynamic responses. The precise impacts of SST, and separately, the thermo and dynamical effects on modulating the AUM must be evaluated in future studies through sensitive experiments using AGCM with prescribed SST and AGCM coupled with a slab ocean.

To assess the robustness of our model response, we further compared our simulation with two equilibrium experiments of CMIP6/PMIP4, the mid-Holocene (6000 years before present, 6 ka BP, MH) and the pre-industrial (AD 1950, PI) experiments. The main external forcing during the MH that differs from the PI is the latitudinal and seasonal distribution of insolation caused by the orbital parameters, especially the precession³². Therefore, the difference between the MH and the PI can be considered to be a good approximation of the response to the precessional forcing. Six

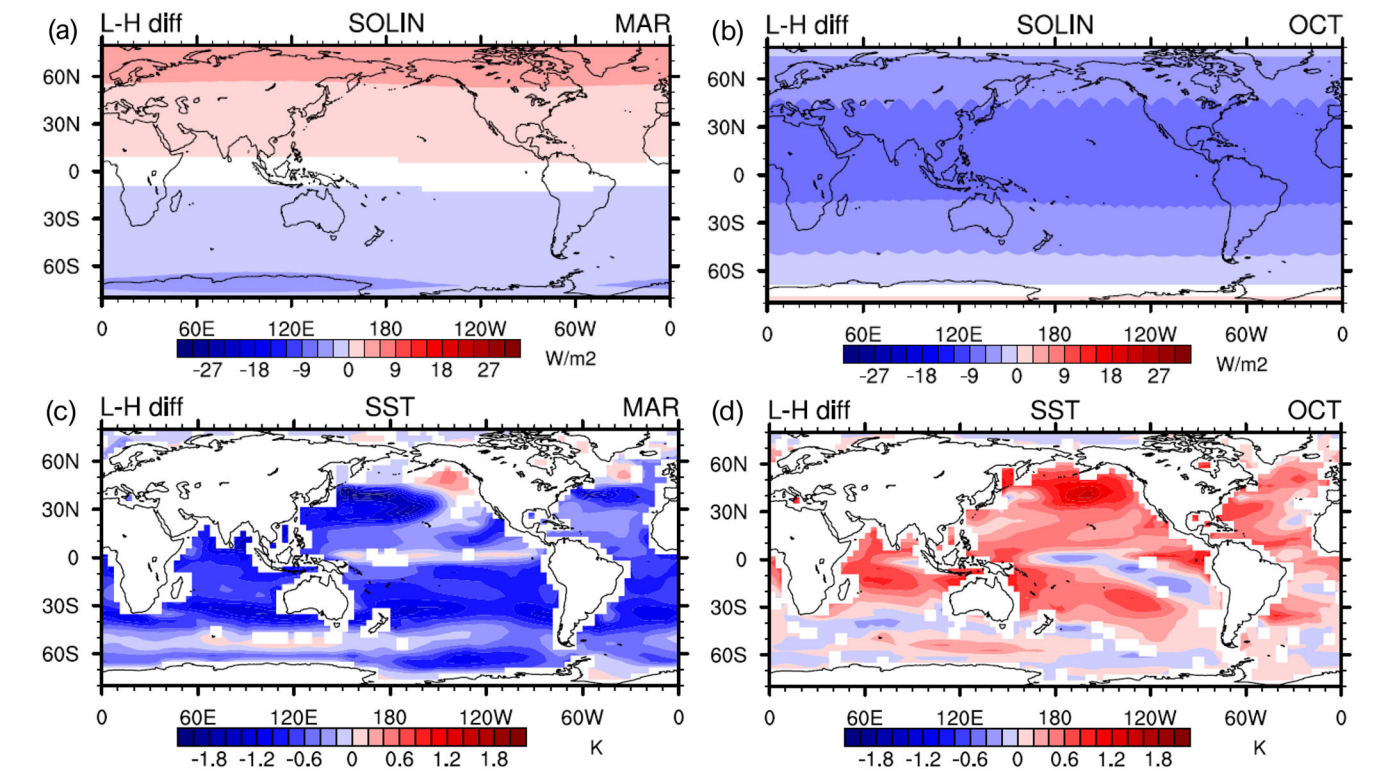


Fig. 6 | Insolation and sea surface temperature changes. Composite maps of (a, b) SOLIN and (c, d) sea surface temperature (SST) anomalies in March (a, c) and October (b, d). The composite anomalies are the differences between low and high precession states. Only those values above 95% confidence level are shown.

Table 2 | CMIP6/PMIP4 models used in this study

Model	Institution	Spatial resolution for atmospheric module Lon*Lat (grids)
FGOALS-g3	Institute of Atmospheric Physics, Chinese Academy of Sciences (IAP CAS), China	180°*80
IPSL-CM6A-LR	Institute Pierre-Simon Laplace (IPSL), France	143°*144
MIROC-ES2L	Japan Agency for Marine–Earth Science and Technology (JAMSTEC), Atmosphere and Ocean Research Institute (AORI), National Institute for Environmental Studies (NIES), and RIKEN Center for Computational Science (R-CCS), Japan	128°*64
MRI-ESM2-0	Meteorological Research Institute (MRI), Japan	320°*160
MPI-ESM1-2-LR	Max Planck Institute for Meteorology (MPI), Germany	192°*96
NESM3	Nanjing University of Information Science and Technology (NUIST), China	192°*96

models are randomly selected in this study to conduct the inter-model comparison (Table 2).

The EASM southerly is stronger and the EASM precipitation is increased in the MH than in PI, robust across the 6 models (Figs. 7 lower panels, 8a). However, most models simulate a weaker AUSM precipitation over the northern Australia. This suggests an anti-phase response to insolation between the EASM precipitation and the AUSM precipitation, consistent with our simulations. On the other hand, all the 6 models simulate strengthened EAWM northerly (Figs. 7 upper panels, 8b). While 4 out of the 6 models simulate weakened AUSM westerly in MH, indicating a weakened dynamical link between the EAWM and the AUSM, consistent with our simulation results.

In comparison with the robust EAM changes across different models, the modeled AUSM here shows some discrepancies from some previous models^{1,31}. This illustrates some uncertainties in simulating the AUM. The uncertainties might come from the model performance in simulating the above-mentioned local oceanic processes, the dynamical vegetation processes, as well as their competition⁸. For example, all six models simulate opposite summer precipitation responses between the Australian continent changes and its adjacent ocean in the northwest (Fig. 7 upper panels), which

is consistent with our simulation (Fig. 2a) and other previous simulations¹. It is, therefore, conceivable that differences in the relative importance of land and oceanic rainfall processes may affect the rainfall in the coastal region of AUSM. Improved models and further experiments are required to fully understand the responses of AUM to orbital forcing.

Our simulated out-of-phase relationship between the EASM intensity, represented by EASM_P, and the AUSM intensity, represented by AUSM_P, at the precession timescale (Figs. 1a, b) is consistent with that between the reconstructed EASM intensity by Cheng et al.²⁴ and the newly reconstructed AUSM intensity by Sarim et al.²¹ (Fig. 1c). The reconstructed AUSM intensity by Pei et al.²⁰, however, doesn't show anti-phase covariances to the reconstructed EASM intensity by Cheng et al.²⁴. We have previously noticed that the AUSM precipitation over the main continent varies oppositely to that over the adjacent ocean at the precession timescale (Figs. 2a, 7 upper panels). Therefore, we suggest that the reconstructed AUSM intensity by Pei et al.²⁰ might indicate the signals over the ocean and that by Sarim et al.²¹ might indicate the signals over the land.

However, linking the record of Pei et al.²⁰ with oceanic precipitation here is somewhat arbitrary because if it reflects the signal of land river runoff, it will not be influenced by rainfall over the ocean. Why Pei et al.²⁰ shows in-

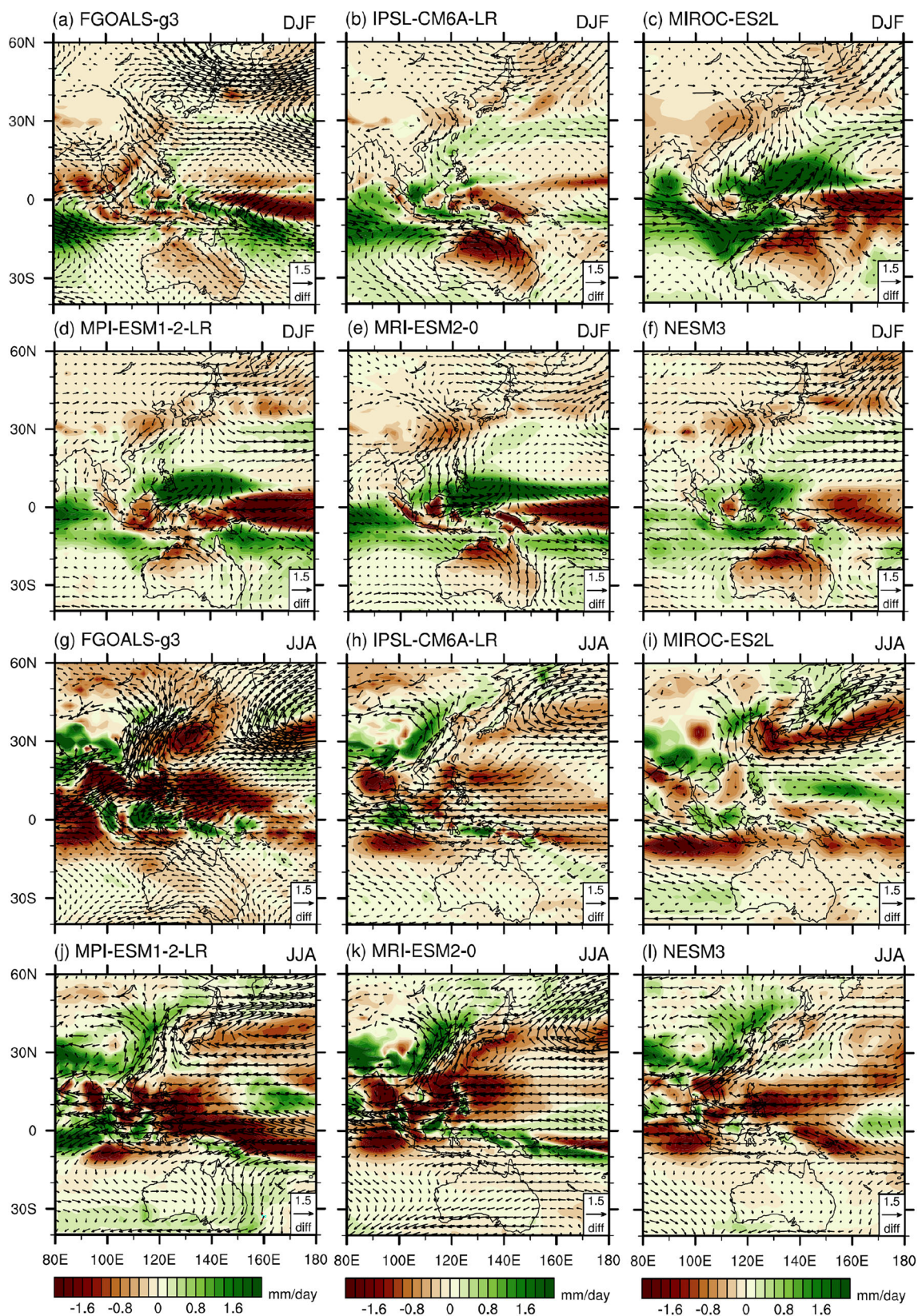


Fig. 7 | Characteristics of low-level circulation and precipitation changes. The differences of the precipitation (shading) and wind field at 850 hPa (vector) in DJF (a–f) and JJA (g–l) between MH and PI. The results are derived from the 6 models contributed to CMIP6/PMIP4.

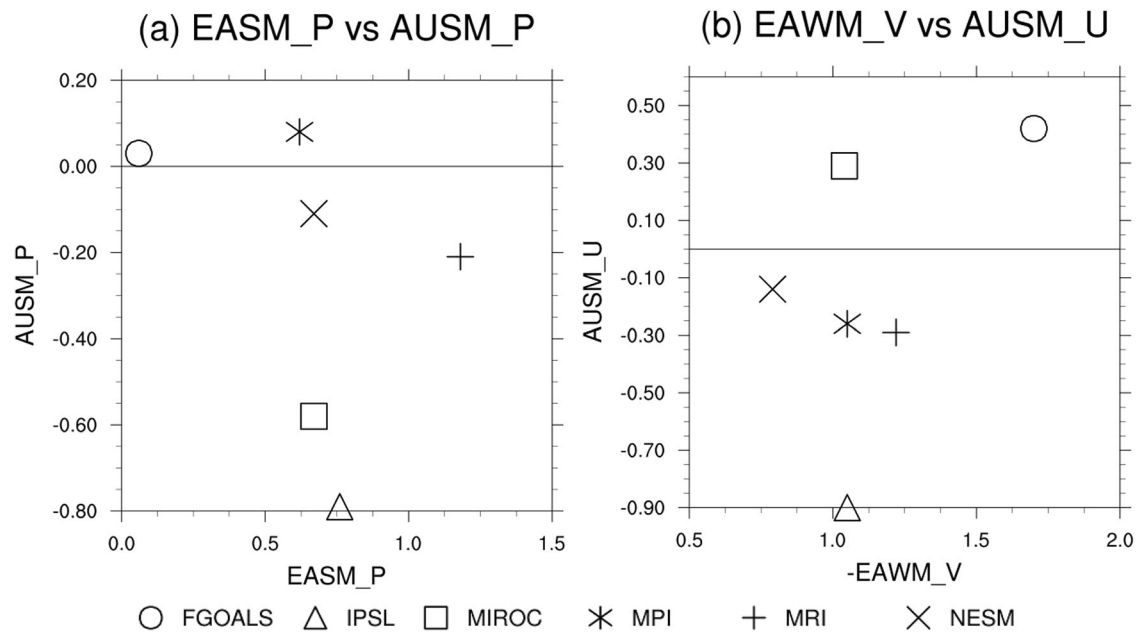


Fig. 8 | Inter-model comparison on EASM-AUSM and EAWM-AUSM relationships. Scatter diagrams of the monsoon precipitation changes (a, EASM_P vs. AUSM_P) and the monsoon circulation changes (b, EAWM_v850 vs. AUSM_u850)

between MH and PI across the six CMIP6/PMIP4 models. The horizontal black lines are the zero lines for AUSM. The positive values indicate increasing and/or strengthening, and vice versa.

phase relationship with Cheng et al.²⁴, as indicated by the relationship between the modeled oceanic precipitation and EASM precipitation, requires further investigations in the future. Furthermore, as mentioned above, although the proxy from Sarim et al.²¹ shows an anti-phase relationship with Cheng et al.²⁴, their correlation coefficient in the precession band is very small and insignificant. We must acknowledge that the proxy records are currently insufficient to support our simulated results. More reconstruction and simulation works are strongly needed to further confirm our hypothesis.

The local insolation and the south-north insolation gradient are considered the primary mechanisms influencing the evolutions of the EAM and AUM, and thereby, the relationship and dynamical linkage between the EAM and AUM. However, changes in remote insolation and local oceanic dynamics may modulate AUM variations and, consequently, impact the EAM-AUM relationship and their dynamic connection. This study finds that AUSM precipitation is affected by local and remote insolation from high latitudes in the Southern Hemisphere, which differs slightly from our previous work²⁸, which indicated significant remote influences from both low latitudes in the Northern Hemisphere and high latitudes in the Southern Hemisphere. Wen et al.²⁸ isolated the impacts of local and remote orbital-induced insolation changes on the EASM and AUSM through four experiments that examined anomalous insolation across the latitude ranges of 90N-45N, 45N-0, 0-45S, and 45S-90S. The experiments were conducted in equilibrium, potentially overlooking the lead/lag effects that are expected given the gradual changes in orbital forcing over time³³. Therefore, further transient sensitivity experiments, following the methodology of Wen et al.²⁸ to isolate local and remote orbital-induced insolation effects but using transient orbital forcing, are necessary in the future to quantify their influences on AUM evolution at orbital timescales.

We should also notice that the correlation coefficient or the coherence does not necessarily illustrate the dynamical links between the EAM and the AUM. The relationship between the NH and SH monsoons mainly indicates their responses to local forcings. More importantly, the summer monsoon precipitation over the Australian land changes differently from that over the adjacent ocean. We should be very careful when comparing the EAM and AUM evolutions at orbital timescales in reconstruction works. Our work may have implications to better understand the monsoon evolutions at orbital timescale.

In summary, this study discussed the evolutionary relationships between the AUSM precipitation and the EASM precipitation at the precession timescale, along with the dynamical links between the AUSM and EAWM circulations. Due to the seasonal and the hemispheric asymmetries, the relationships and the links show different responses in different seasons. The precession-induced local insolation change plays a dominant role in deciding the “out-of-phase” relationship between the AUSM and the EASM. And the AUSM - EAWM dynamical linkage can be “weakened” or even “cut off” by the south-north insolation gradient change in response to precession. Future studies are still needed to reduce discrepancies on identifying the relationship between AUSM and EASM/EAWM from both model and proxy perspectives.

Methods

Simulation data

The experiments used in this study are a set of accelerated transient simulations spanning the past 300,000 years (300 kyrs), conducted with the National Center for Atmospheric Research Community Climate System Model version 3 (NCAR-CCSM3)²³. The results are derived mainly from the pure orbital run (ORB), which is forced only by the transient orbital parameters. The other experiment (OGG) is also used to evaluate the model performance. It is forced by the transient orbital parameters, the greenhouse gases, and the ice sheet. The transient orbital parameters and the greenhouse gases concentrations are accelerated by a factor of 100 (advanced by 100 years of changes in real time at the end of each model year). The past 300,000 years climate evolution is then represented in these 3000-model-year-long transient simulations. Since the response time of the upper ocean is faster than the precession period, the upper ocean has time to fully adjust to the accelerated forcing and showed quasi-equilibrium response³⁴⁻³⁶. Lorenz and Lohmann³⁷ also found that the differences in using 10 and 100 acceleration factors were insignificant for surface climate variables. In this study, we restrict to analysis of the responses of the upper ocean and the surface climate, where the acceleration is justified. Specifically, if we compare the EASM_v850 during the last 21 kyrs in this accelerated simulation to that in the unaccelerated transient simulation of the last 21 kyrs (TRACE-21ka)¹¹, they show similar evolutionary characteristics.

In addition, to avoid the artificial phase shift in the monthly insolation and the monthly climate response, the monthly model output with “fixed-

day” calendar was converted to the monthly data with “fixed-angular” calendar, based on Bartlein and Shafer³⁸.

Proxy data

To evaluate the model results, three proxy-based monsoon indices are collected. The composite $\delta^{18}\text{O}$ from Chinese caves over the last 640 kyrs is used to represent the EASM intensity²⁴. The kaolinite/smectite ratios from the IODP high sedimentation Site U1483 off the Scott Plateau of the northwest Australian margin are adopted as the proxy for the AUSM²¹. Another terrigenous sedimentation along the northwestern Australian margin, the monsoonal discharge²⁰ ($\text{Log}(\text{Terr}/\text{Ca})$) in the composite record from core SO157-18548 and IODP site U1482, is also collected to represent AUSM intensity.

Data availability

The accelerated ORB and OGG output are available from the corresponding author upon reasonable request. The CMIP6-PMIP4 output dataset can be accessed through the official CMIP6 channels via the Earth System Grid Federation (ESGF; <https://earthsystemcog.org/projects/wip/CMIP6DataRequest>). The composite $\delta^{18}\text{O}$ reconstructed by Cheng et al. (2016) is available via the National Centers for Environmental Information (NCEI), National Oceanic and Atmospheric Administration (NOAA; <https://www.ncei.noaa.gov/access/paleo-search/>). The clay minerals data collected by Sarim et al. (2023) is available via their Zenodo database (<https://doi.org/10.5281/zenodo.7418088>). The monsoonal discharge ($\text{Log}(\text{Terr}/\text{Ca})$) data is downloaded from their online version (<https://doi.org/10.1016/j.palaeo.2021.110280>).

Code availability

The source codes for the analysis of this study are available from the corresponding author upon reasonable request.

Received: 15 September 2024; Accepted: 7 May 2025;

Published online: 20 May 2025

References

- Liu, Z. et al. Coupled climate simulation of the evolution of global monsoon in the Holocene. *J. Clim.* **16**, 2472–2490 (2003).
- Ding, R., Ha, K.-J. & Li, J. Interdecadal shift in the relationship between the East Asian summer monsoon and the tropical Indian Ocean. *Clim. Dyn.* **34**, 1059–1071 (2010).
- Matsumoto, J. The Seasonal Changes in Asian and Australian Monsoon Regions. *J. Meteorol. Soc. Jpn. Ser. II* **70**, 257–273 (1992).
- Eroglu, D. et al. “See-saw relationship of the Holocene East Asian-Australian summer monsoon.”. *Nat. Commun.* **7**, 12929 (2016).
- Zhang, J. et al. “Asian-Australian monsoon evolution over the last millennium linked to ENSO in composite stalagmite $\delta^{18}\text{O}$ records.”. *Quat. Sci. Rev.* **281**, 107420 (2022).
- Xu, C. et al. “Asian-Australian summer monsoons linkage to ENSO strengthened by global warming. *npj Clim. Atmos. Sci.* **6**, 8 (2023).
- Magee, J. W., Miller, G. H., Spooner, N. A. & Questiaux, D. Continuous 150 k.y. monsoon record from Lake Eyre, Australia: Insolation-forcing implications and unexpected Holocene failure. *Geology* **32**, 885 (2004).
- Miller, G. et al. Sensitivity of the Australian Monsoon to insolation and vegetation: Implications for human impact on continental moisture balance. *Geology* **33**, 65 (2005).
- Wang, P. X. et al. The global monsoon across timescales: coherent variability of regional monsoons. *Climate* **10**, 2007–2052 (2014).
- Wang, P. X. et al. The global monsoon across time scales: Mechanisms and outstanding issues. *Earth-Sci. Rev.* **174**, 84–121 (2017).
- Wen, X. et al. Correlation and anti-correlation of the East Asian summer and winter monsoons during the last 21,000 years. *Nat. Commun.* **7**, 11999 (2016).
- Müller, U. C., Fletcher, W. J., Milner, A. M. & Scheiter, S. Interhemispheric anti-phasing of orbitally driven monsoon intensity: Implications for ice-volume forcing in the high latitudes. *Earth Planet. Sci. Lett.* **377–378**, 34–42 (2013).
- Webster, P. J. et al. Monsoons: Processes, predictability, and the prospects for prediction. *J. Geophys. Res.: Oceans* **103**, 14451–14510 (1998).
- Clemens, S. C. Southern Hemisphere forcing of Pliocene $\delta^{18}\text{O}$ and the evolution of Indo-Asian monsoons. *Paleoceanography* **23**, PA4210 (2008).
- Sun, Y. B. Seven million years of wind and precipitation variability on the Chinese Loess Plateau. *Earth Planet. Sci. Lett.* **297**, 525–535 (2010).
- Yan, M., Liu, Z. Y., Ning, L. & Liu, J. Holocene EASM-EAWM Relationship Across Different Timescales in CCSM3. *Geophys. Res. Lett.* **47**, e2020GL088451 (2020).
- Yan, M. et al. Relationship between the East Asian Summer and Winter Monsoons at Obliquity Time Scales. *J. Clim.* **36**, 3993–4003 (2023).
- Jalilhal, C., Bosmans, J. H. C., Srinivasan, J. & Chakraborty, A. The response of tropical precipitation to Earth’s precession: the role of energy fluxes and vertical stability. *Climate* **15**, 449–462 (2019).
- Gong, L. et al. Middle Pleistocene re-organization of Australian Monsoon. *Nat. Commun.* **14**, 2002 (2023).
- Pei, R. et al. Monitoring Australian Monsoon variability over the past four glacial cycles. *Palaeogeogr., Palaeoclimatol., Palaeoecol.* **568**, 110280 (2021).
- Sarim, M. et al. Late quaternary clay mineral and grain-size records from northwest Australia and their implications for paleoclimate, ocean currents, and paleodrainage of the Bonaparte basin. *Palaeogeogr., Palaeoclimatol., Palaeoecol.* **610**, 111353 (2023).
- Weij, R. et al. Elevated Southern Hemisphere moisture availability during glacial periods. *Nature* **626**, 319–326 (2024).
- Lu, Z. et al. Prominent precession band variance in ENSO intensity over the last 300,000 years. *Geophys. Res. Lett.* **46**, 9786–9795 (2019).
- Cheng, H. et al. The Asian monsoon over the past 640,000 years and ice age terminations. *Nature* **534**, 640–646 (2016).
- Wang, X. et al. “Millennial-scale precipitation changes in southern Brazil over the past 90,000 years.”. *Geophys. Res. Lett.* **34**, L23701 (2007).
- Tachikawa, K. et al. The precession phase of hydrological variability in the Western Pacific Warm Pool during the past 400 ka. *Quat. Sci. Rev.* **30**, 3716–3727 (2011).
- Wang, Y. et al. Millennial- and orbital-scale changes in the East Asian monsoon over the past 224,000 years. *Nature* **451**, 1090–1093 (2008).
- Wen, Q., Yan, M., Liu, Z. & Liu, J. Responses of East Asian Winter Monsoon-Australian Summer Monsoon to Local and Remote Orbital Forcing During Holocene. *Geophys. Res. Lett.* **49**, e2022GL098865 (2022a).
- Wen, Q. et al. Local Insolation Drives Afro-Asian Monsoon at Orbital-Scale in Holocene. *Geophys. Res. Lett.* **49**, e2021GL097661 (2022b).
- Dai, A., Zhao, T. & Chen, J. Climate Change and Drought: a Precipitation and Evaporation Perspective. *Curr. Clim. Change Rep.* **4**, 301–312 (2018).
- Wyrwoll, K.-H. et al. Sensitivity of the Australian summer monsoon to tilt and precession forcing. *Quat. Sci. Rev.* **26**, 3043–3057 (2007).
- Otto-Bliesner, B. L. et al. The PMIP4 contribution to CMIP6 – Part 2: Two interglacials, scientific objective and experimental design for Holocene and Last Interglacial simulations. *Geoscientific Model Dev.* **10**, 3979–4003 (2017).
- Kutzbach, J. E., Liu, X., Liu, Z. & Chen, G. Simulation of the evolutionary response of global summer monsoons to orbital forcing over the past 280,000 years. *Clim. Dyn.* **30**, 567–579 (2008).
- Jackson, C. S. & Broccoli, A. J. Orbital forcing of Arctic climate: mechanisms of climate response and implications for continental glaciation. *Clim. Dyn.* **21**, 539–557 (2003).

35. Timmermann, A., Lorenz, S. J., An, S. I., Clement, A. & Xie, S. P. The Effect of Orbital Forcing on the Mean Climate and Variability of the Tropical Pacific. *J. Clim.* **20**, 4147–4159 (2007).
36. Kutzbach, J. E. et al. African climate response to orbital and glacial forcing in 140,000-y simulation with implications for early modern human environments. *Proc. Natl Acad. Sci. USA* **117**, 2255–2264 (2020).
37. Lorenz, S. J. & Lohmann, G. Acceleration technique for Milankovitch type forcing in a coupled atmosphere-ocean circulation model: method and application for the Holocene. *Clim. Dyn.* **23**, 727–743 (2004).
38. Bartlein, P. J. & Shafer, S. L. “Paleo calendar-effect adjustments in time-slice and transient climate-model simulations (PaleoCalAdjust v1.0): Impact and strategies for data analysis.”. *Geosci. Model Dev.* **12**, 3889–3913 (2019).

Acknowledgements

This work is jointly supported by the Program of Global Change and Mitigation, the Ministry of Science and Technology of China (2023YFF0804704), the Science and Technology Innovation Project of Laoshan Laboratory (Grant LSKJ202203303), the National Natural Science Foundation of China (Grants 42475051, 42130604, 42075049, 41971021), and the Priority Academic Program Development of Jiangsu Higher Education Institutions (Grant 164320H1813).

Author contributions

M.Y. & Z.L.: Conceptualization, Data, Investigation, Analysis, Writing Original draft, Reviewing, Editing. B.W.: Analysis, Reviewing, Editing. X.K.: Methodology, Visualization. N.L. & Q.W.: Reviewing, Editing. J.L.: Reviewing, Editing, Supervision.

Competing interests

The authors declare no competing interests.

Additional information

Supplementary information The online version contains supplementary material available at <https://doi.org/10.1038/s41612-025-01084-y>.

Correspondence and requests for materials should be addressed to Jian Liu.

Reprints and permissions information is available at <http://www.nature.com/reprints>

Publisher's note Springer Nature remains neutral with regard to jurisdictional claims in published maps and institutional affiliations.

Open Access This article is licensed under a Creative Commons Attribution-NonCommercial-NoDerivatives 4.0 International License, which permits any non-commercial use, sharing, distribution and reproduction in any medium or format, as long as you give appropriate credit to the original author(s) and the source, and provide a link to the Creative Commons license. You do not have permission under this license to share adapted material derived from this article or parts of it. The images or other third party material in this article are included in the article's Creative Commons license, unless indicated otherwise in a credit line to the material. If material is not included in the article's Creative Commons license and your intended use is not permitted by statutory regulation or exceeds the permitted use, you will need to obtain permission directly from the copyright holder. To view a copy of this license, visit <http://creativecommons.org/licenses/by-nc-nd/4.0/>.

© The Author(s) 2025